Behavioral/Systems/Cognitive

Inositol 1,4,5-Trisphosphate-Dependent Ca^{2+} Threshold Dynamics Detect Spike Timing in Cerebellar Purkinje Cells

Tomokazu Doi,[1,2] **Shinya Kuroda,**[3,4] **Takayuki Michikawa,**[5] **and Mitsuo Kawato**[1]

[1]ATR Computational Neuroscience Laboratories, Kansai Science City, Kyoto 619-0288, Japan, [2]Graduate School of Information Science, Nara Institute of Science and Technology, Ikoma-shi, Nara 630-0192, Japan, [3]Undergraduate Program for Bioinformatics and Systems Biology, Graduate School of Information Science and Technology, The University of Tokyo, Bunkyo-ku, Tokyo 113-0033, Japan, [4]Precursory Research for Embryonic Science and Technology, Japan Science and Technology, Bunkyo-ku, Tokyo 113-0033, Japan, and [5]Division of Molecular Neurobiology, Department of Basic Medical Science, Institute of Medical Science, The University of Tokyo, Minato-ku, Tokyo 108-8639, Japan

Large Ca^{2+} signals essential for cerebellar long-term depression (LTD) at parallel fiber (PF)–Purkinje cell synapses are known to be induced when PF activation precedes climbing fiber (CF) activation by 50–200 ms, consistent with cerebellar learning theories. However, large Ca^{2+} signals and/or LTD can also be induced by massive PF stimulation alone or by photolysis of caged Ca^{2+} or inositol 1,4,5-trisphosphate (IP_3). To understand the spike-timing detection mechanisms in cerebellar LTD, we developed a kinetic model of Ca^{2+} dynamics within a Purkinje dendritic spine. In our kinetic simulation, IP_3 was first produced via the metabotropic pathway of PF inputs, and the Ca^{2+} influx in response to the CF input triggered regenerative Ca^{2+}-induced Ca^{2+} release from the internal stores via the IP_3 receptors activated by the increased IP_3. The delay in IP_3 increase caused by the PF metabotropic pathway generated the optimal PF–CF interval. The Ca^{2+} dynamics revealed a threshold for large Ca^{2+} release that decreased as IP_3 increased, and it coherently explained the different forms of LTD. At 2.5 μM IP_3, CF activation after PF activation was essential to reach the threshold for the regenerative Ca^{2+} release. At 10 μM IP_3, the same as achieved experimentally by strong IP_3 photolysis, the threshold was lower, and thus large Ca^{2+} release was generated even without CF stimulation. In contrast, the basal 0.1 μM IP_3 level resulted in an extremely high Ca^{2+} threshold for regenerative Ca^{2+} release. Thus, the results demonstrated that Ca^{2+} dynamics can detect spike timing under physiological conditions, which supports cerebellar learning theories.

Key words: **calcium; LTD; simulation; timing detection; inositol; feedback**

Introduction

The Purkinje cells in the cerebellar cortex receive two major excitatory synaptic inputs, one of which is from a number of parallel fibers (PFs) and the other of which is from a single climbing fiber (CF). Cerebellar long-term depression (LTD) is a persistent reduction in the efficacy of PF–Purkinje cell synapses that is induced by paired stimulation of PFs and CFs, and it is thought to be one of the cellular bases of learning and memory (Marr, 1969; Albus, 1971; Linden and Connor, 1995; Ito, 2001). Cerebellar learning theories (Ito, 1970; Kawato, 1999; Yamamoto et al., 2002) state that PFs convey the information required for motor command generation, whereas CFs carry error signals, which are inevitably delayed compared with PF activation. Thus, the theories predict that PF activation preceding CF activation is a more effective sequence to induce LTD than CF activation preceding PF activation, and this has been supported by several experimental studies (Chen and Thompson, 1995; Schreurs et al., 1996; Wang et al., 2000). However, inconsistent PF–CF time windows for LTD induction have frequently been reported, and it has been found possible to induce LTD *in vitro* by massive stimulation of a PF bundle alone (Hartell, 1996), Ca^{2+} uncaging (Miyata et al., 2000), or inositol 1,4,5-trisphosphate (IP_3) uncaging (Finch and Augustine, 1998) instead of by conjunctive PF–CF stimulation, thus raising doubts about LTD as one of the cellular bases of learning (De Schutter, 1995; Llinas et al., 1997).

Among the many signaling molecules involved in LTD induction, Ca^{2+} has been suggested as a candidate for the molecule that detects the coincidence and the timing of PF- and CF-induced spikes in Purkinje cell dendrites (Berridge, 1998; Wang et al., 2000). Multiphoton Ca^{2+} imaging of dendritic spines in Purkinje cells has shown that PF stimulation followed by CF stimulation is the most efficient sequence for inducing "supralinear" Ca^{2+} signals (>10 μM) and subsequent cerebellar LTD (Wang et al., 2000). The term "supralinear" means that the Ca^{2+} response to conjunctive PF–CF inputs is greater than the sum of the responses to PF input alone and CF input alone. The IP_3 receptor (IP_3R) is a possible candidate for the coincidence detector for supralinear Ca^{2+} increases (Berridge, 1998). IP_3Rs are intracellular Ca^{2+} release channels that are coactivated by IP_3 and Ca^{2+}, and they are essential for the induction of LTD (Finch and Augustine, 1998; Inoue et al., 1998). Although PF inputs induce

Received July 8, 2004; revised Dec. 3, 2004; accepted Dec. 4, 2004.

This work was supported by the Human Frontier Science Program (M.K.) and the National Institute of Information and Communications Technology.

Correspondence should be addressed to Tomokazu Doi, ATR Computational Neuroscience Laboratories, 2-2-2 Hikaridai, Kansai Science City, Kyoto 619-0288, Japan. E-mail: xtomdoi@atr.jp.

DOI:10.1523/JNEUROSCI.2727-04.2005

 0270-6474/05/250950-12$15.00/0

production of IP_3 via the metabotropic pathway (Finch and Augustine, 1998), CF input induces strong depolarization leading to a Ca^{2+} influx through voltage-gated Ca^{2+} channels (VGCCs) of Purkinje cell dendrites at PF spines (Miyakawa et al., 1992). However, the idea that IP_3Rs constitute the mechanism for coincidence detection needs to be further explored and tested to determine whether it is capable of explaining the temporal window and the different forms of LTD.

To elucidate the dynamics of the cellular computations for spike-timing detection, we developed a Ca^{2+} dynamics model based on known biochemical signal transduction pathways. We first hypothesized that a delay in the increase in IP_3 caused by the PF metabotropic pathway generates the optimal PF–CF interval, that CF input after PF input triggers regenerative Ca^{2+} release from internal stores through IP_3Rs, and that the Ca^{2+} response exhibited a threshold dynamics for large Ca^{2+} release that decreases as IP_3 increases. If this hypothesis is true, it would coherently explain the different forms of LTD.

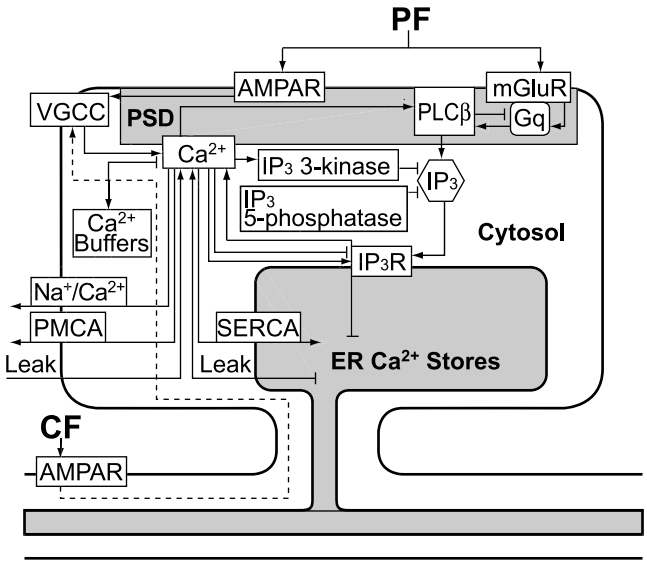

Figure 1. Block diagram of signaling pathways for Ca^{2+} release at a dendritic spine in Purkinje cells. Arrows and bars indicate stimulatory and inhibitory interactions. The dashed arrow indicates depolarization by CF stimulation. Molecular diffusion through the spine neck is not considered.

Materials and Methods

Model structure and compartments of a Purkinje dendritic spine

We modeled a mature Purkinje dendritic spine and divided it into three compartments [i.e., the cytosol, postsynaptic density (PSD), and endoplasmic reticulum (ER), with volumes of 0.1, 0.002, and 0.02 μm^3, respectively] based on serial electron microscopy observations (Harris and Stevens, 1988), and the volume of the extracellular space was 10 μm^3. Because of the small volume of the spine, we assumed that the molecules it contains were well mixed and that their concentrations were uniform within each compartment. All spatial diffusion of molecules between compartments is mediated by channels and pumps, except for the diffusion of IP_3 and Ca^{2+} between the cytosol and PSD. The diffusion constants of the molecules are so high [the diffusion constants are 283 $\mu m^2/s$ for IP_3 (Allbritton et al., 1992) and 220 $\mu m^2/s$ for Ca^{2+} (Klingauf and Neher, 1997)] that diffusion between compartments in the small volume of the spine should be completed within 1 ms. We therefore set that the concentrations of IP_3 and Ca^{2+} would reach a state of dynamic equilibrium between the cytosol and PSD with a time constant of 1 ms, which is much faster than most chemical binding reactions in Ca^{2+} signaling.

We did not model the Ca^{2+} concentration in the dendritic shafts or soma because dendritic spines are biochemically almost completely separated from their dendrites. Ca^{2+} ions in the spines do not diffuse much through the spine neck (Sabatini et al., 2002). Because cerebellar Purkinje cells contain higher concentrations of endogenous Ca^{2+} buffers than other neurons (Fierro and Llano, 1996; Maeda et al., 1999), for the sake of simplicity, all Ca^{2+} entry from outside the spine can be assumed to be attributable to Ca^{2+} influx from VGCCs at the spine. Because action potential activity in the soma does not propagate back to dendritic shafts and spines in Purkinje cells (Stuart and Hausser, 1994; Vetter et al., 2001), Ca^{2+} influx in the spine is mainly induced by PF and CF activation. We applied Ca^{2+} pulse as Ca^{2+} influx by PF and CF activation instead of by modeling the kinetics of AMPARs and VGCCs. Although dense PF stimulation induces large Ca^{2+} influxes (Wang et al., 2000), we did not apply dense bundle PF stimulation. Ca^{2+} influx induced by repetitive PF activation may be strengthened or weakened because of depolarization and/or hyperpolarization as a result of the activity of other synapses, but we ignored the effects of other synaptic activity as well as short-term potentiation or depression in our model.

Block diagram of Ca^{2+} signaling pathways

We constructed a block diagram of Ca^{2+} signal transduction pathways in a Purkinje dendritic spine (Fig. 1), based on the literature (Fiala et al., 1996; Kim and Thompson, 1997; Daniel et al., 1998; Rose and Konnerth, 2001; Ito, 2002). CF input generates a strong depolarization and opens VGCCs, resulting in a Ca^{2+} influx into the dendritic spine (Miyakawa et al., 1992). PF input raises the postsynaptic Ca^{2+} concentration in the Purkinje dendritic spine via two pathways, one mediated by AMPA receptors (AMPARs) and the other mediated by metabotropic glutamate receptors (mGluRs). In the AMPAR pathway, the activated AMPARs induce depolarization of the membrane potential of the PF spine and open VGCCs (Eilers et al., 1995), and extracellular Ca^{2+} enters the cytosol through the VGCCs. In the mGluR pathway, glutamate released from the PF terminal activates mGluRs, and the activated mGluRs in turn induce production of IP_3 via G-proteins (Gq) and phospholipase Cβ (PLCβ) at the PSD (Jiang et al., 1994; Sugiyama et al., 1999; Tanaka et al., 2000). IP_3 then diffuses from the postsynaptic membrane into the cytosol. Finally, IP_3Rs, which are IP_3-gated Ca^{2+} channels in the ER, release Ca^{2+} from the ER (Finch and Augustine, 1998).

Cytosolic IP_3 is degraded by IP_3 3-kinase and IP_3 5-phosphatase within a few seconds (Dupont and Erneux, 1997; Irvine and Schell, 2001). Free cytosolic Ca^{2+} is buffered by Ca^{2+} endogenous buffers, and we included parvalbumin, calbindin-D_{28k}, and putative low-affinity buffers (Airaksinen et al., 1997; Maeda et al., 1999; Vecellio et al., 2000). We also included an exogenous buffer, Magnesium Green 1 as a Ca^{2+} indicator, to compare the results of simulation with the results of the Ca^{2+} imaging experiments (Wang et al., 2000). Cytosolic Ca^{2+} is pumped out by Na^+/Ca^{2+} exchangers and Ca^{2+}-ATPase in the plasma membrane (PMCA) and in the ER (SERCA) (Xu et al., 1997).

Representation of PF and CF inputs in the model

Instead of modeling the kinetics of AMPARs and VGCCs, a rectangular Ca^{2+} pulse was applied to the cytosol to achieve a Ca^{2+} influx as a result of VGCC opening. Instead of the CF input, an influx of 5000 Ca^{2+} ions was delivered over a period of 2 ms (in the form of a rectangular Ca^{2+} entry waveform with 2500 ions/ms). PF input was represented by a burst consisting of five pulses at 100 Hz. Instead of the AMPAR pathway, an influx of 1500 Ca^{2+} ions over a period of 1 ms per PF pulse was delivered. This assumed degree of Ca^{2+} influx is consistent with a previous estimate that the Ca^{2+} influx through VGCCs in the spines is ~1000 Ca^{2+} ions per depolarization (Sabatini and Svoboda, 2000). Glutamate was released at the synaptic cleft during each PF pulse. Only 300 glutamate molecules were assumed to be involved in the binding reaction of Glu and mGluRs, because mGluRs localize at the edge of the PSD, where the neurotransmitter concentration is lower than at the center of the PSD (Mateos et al., 2000; Franks et al., 2003). The glutamate was recycled by glutamate transporters with a decaying time constant of 5 ms.

Formulation of the reactions in the signaling pathways

All reactions in the signal transduction pathways were represented by binding and enzymatic reactions. For example, a binding reaction in which *A* binds to *B* to form *AB* is expressed by the following equation:

$$A + B \underset{k_b}{\overset{k_f}{\rightleftarrows}} AB, \quad (1)$$

where k_f and k_b are the rate constants for the forward and backward reactions. The rates k_f and k_b are determined by the dissociation constant K_d and the time constant τ. K_d is defined as $K_d = k_b/k_f$. τ indicates the reaction speed toward the equilibrium. Equation 1 is represented as a differential equation with the following form:

$$d[AB]/dt = k_f[A][B] - k_b[AB]. \quad (2)$$

Enzymatic reactions were modeled by the Michaelis–Menten formulation:

$$S + E \underset{k_{-1}}{\overset{k_1}{\rightleftarrows}} SE \xrightarrow{k_{cat}} P + E, \quad (3)$$

where *S*, *E*, and *P* denote substrates, enzymes, and products, respectively. The Michaelis constant K_m is defined as $K_m = (k_{-1} + k_{cat})/k_1$. The maximum enzyme velocity V_{max} is defined as $V_{max} = k_{cat}[E]_{total}$, where $[E]_{total}$ is the total concentration of the enzyme. Unless actual rate constants were provided in the literature, k_{-1} was assumed to be four times larger than k_{cat}. Additional simulations confirmed that the ratio of k_{-1} to k_{cat} had little effect on the Ca^{2+} response. Graphic illustrations of all reactions are provided in supplemental Figure 1 (available at www.jneurosci.org as supplemental material). Details regarding parameter estimation, kinetic reactions, and the parameter table in the model are given in supplemental Tables 1 and 2 (available at www.jneurosci.org as supplemental material).

Schematic model of IP_3R kinetics

We constructed a model of IP_3R kinetics based on recent measurements of Ca^{2+} release (Marchant and Taylor, 1997) and a conceptual model (Adkins and Taylor, 1999). It was assumed that each IP_3R possesses one IP_3 activation site, one Ca^{2+} activation site, and four Ca^{2+} inactivation sites. IP_3 binding determines whether a Ca^{2+} ion binds to the activation site or to one of the four inactivation sites in the model (Fig. 2*A*). In the basal state, 90% of IP_3Rs are not bound to any ligands (Fig. 2*A*, R). IP_3 binding to an IP_3R exposes the Ca^{2+} activation site. Thus, IP_3R opening requires sequential binding to one IP_3 molecule and one Ca^{2+} ion (Fig. 2*A*, R→RI→RIC). On the other hand, if no IP_3 binds to an IP_3R, the four Ca^{2+} inactivation sites are exposed, and binding of one or more Ca^{2+} ions to the inactivation sites of an IP_3R prevents IP_3 binding to the IP_3 activation site (Fig. 2*A*,*B*, R→RC→RC2→RC3→RC4) (Marchant and Taylor, 1997; Adkins and Taylor, 1999). The IP_3R model reproduced the equilibrium open probability of an IP_3R that possesses a bell-shaped Ca^{2+} dependency with a peak free cytosolic Ca^{2+} concentration ($[Ca^{2+}]_i$) of 0.2–0.3 μM (Bezprozvanny et al., 1991; Fujiwara et al., 2001). The numbers of Ca^{2+} activation and inactivation sites influence the steepness of this open-probability function, and a curve fitting the bell-shaped open-probability function helped us to recognize that the existence of one activation site and four inactivation sites in an IP_3R satisfied the experimental data (Fig. 2*C*). The number of inactivation sites is consistent with the fact that an IP_3R consists of four identical subunits.

Estimation of kinetic parameters in the IP_3R model

Biochemical reactions are generally characterized by two parameters, a forward rate constant (k_f) and a backward rate constant (k_b), and we estimated the dissociation constant K_d and time constant τ, which uniquely determine the value of k_f and k_b.

IP_3-dependent activation. Distinct affinities of IP_3R for IP_3 have been reported in *in vitro* and *in vivo* measurements. A purified IP_3R in the constituted lipid bilayer showed the affinity K_d for IP_3 of ~1 μM (Bezprozvanny et al., 1991), whereas Ca^{2+} response to photolysis of caged IP_3 in Purkinje cells suggested lower affinity of IP_3R for IP_3, because IP_3-induced Ca^{2+} release required an IP_3 concentration >10 μM (Khodakhah and Ogden, 1995). From other *in vivo* measurements of IP_3R-mediated Ca^{2+} depletion of the Ca^{2+} stores, the K_d value was estimated to be 25.8 μM (Fujiwara et al., 2001), and we used this value. IP_3 binding must be slow to explain the delay of 50–400 ms in Ca^{2+} release in response to IP_3 application, suggested in other *in vivo* measurements (Marchant and Taylor, 1997). In contrast, our model with rapid IP_3 binding reproduced the delay in Ca^{2+} release (see Fig. 8*C*, right, black), and the delay resulted from a positive feedback of Ca^{2+}-induced Ca^{2+} release. Because IP_3R opening requires coactivation by Ca^{2+} and IP_3, IP_3 application alone does not instantaneously and fully activate Ca^{2+} release through IP_3Rs.

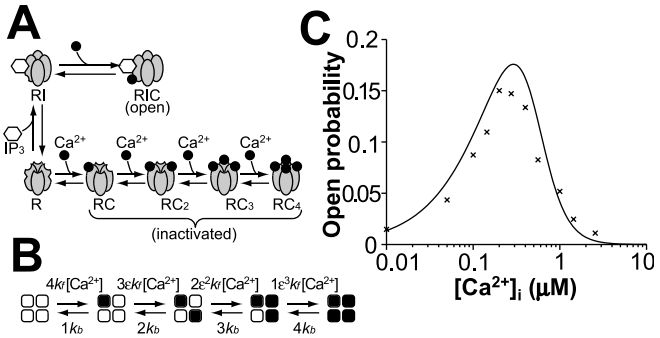

Figure 2. Model of IP_3R kinetics used in the simulation. *A*, Most IP_3Rs are not bound to any ligands (R) in the steady state. Both IP_3 and Ca^{2+} are required to open IP_3Rs. The Ca^{2+} activation site does not emerge until IP_3 binds to the IP_3R. An IP_3R opens when IP_3 binds to the IP_3R and then Ca^{2+} binds to the IP_3R (R⟶RI⟶RIC). Ca^{2+} also inactivates IP_3Rs (R⟶RC⟶RC2⟶RC3⟶RC4). IP_3 cannot bind to IP_3Rs in any of these four inactivation states. IP_3Rs are activated and then inactivated by Ca^{2+} elevation, because the inactivation of IP_3Rs by Ca^{2+} is assumed to be much slower than the activation of IP_3Rs by Ca^{2+} for positive feedback loop of Ca^{2+}-induced Ca^{2+} release. *B*, Parameter reduction during the process of IP_3R inactivation by Ca^{2+} binding. White and black squares indicate naive and inactivated subunits, respectively, of an IP_3R. The eight parameters in the IP_3R inactivation kinetics are reduced to three parameters: k_f, k_b, and ϵ. *C*, Open probability of IP_3Rs dependent on cytosolic Ca^{2+} concentration (line) in the model at 10 μM IP_3 and x in experiments with IP_3Rs reconstituted into planar lipid bilayers at 2 μM IP_3 (Bezprozvanny et al., 1991). The difference in the IP_3 concentrations is attributable to the lower IP_3 affinity of IP_3Rs *in vivo* than in the constructed lipid bilayers (Khodakhah and Ogden, 1995; Fujiwara et al., 2001).

Ca^{2+}-dependent activation. The dissociation constant K_d was estimated from the bell-shaped Ca^{2+}dependency measured by both the open probability in lipid bilayers (Bezprozvanny et al., 1991) and the Ca^{2+} release *in vivo* (Fujiwara et al., 2001). We assumed that the activation is fast ($\tau < 10$ ms), because no studies have reported the speed of Ca^{2+} activation.

Ca^{2+}-dependent inactivation. We assumed a multiple-step model for Ca^{2+}-dependent inactivation, because multiple steps are required to reproduce the full inactivation of IP_3Rs at high Ca^{2+} concentrations (Bezprozvanny et al., 1991; Fujiwara et al., 2001). The four inactivation sites are identical (i.e., only the number of inactivation sites occupied by Ca^{2+} ions affects the sequential inactivation reactions, without regard to the actual positions occupied). The Ca^{2+}-binding reactions to the four inactivation sites are governed by a total of eight parameters [four forward rate constants (k_f) and four backward constants (k_b), or four dissociation constants (K_d) and four time constants (τ)] (see Fig. 2*B*). For simplification, we assumed that binding of one additional Ca^{2+} ion increases the k_f value ϵ-fold (ϵ is referred to as the "cooperative factor"). If $\epsilon = 1$, the inactivation reaction of each subunit is independent of the state of the other subunits. Note that this simplification is used just to reduce the parameter number and has not been experimentally confirmed.

Simplification reduced the eight parameters to three parameters (k_f, k_b, and ϵ). Curve fitting to the bell shape (Fig. 2*C*) yielded $k_b/k_f = 2.25$ μM and $\epsilon = 3$. The time constant τ was estimated ($k_f = 2.22$/s/μM, $k_b = 5$/s)

Table 1. Classification of parameters

Classes of parameters	Known				Unknown	Total
	From Purkinje cells	From other cells	From reactions in test tubes	From other molecular subtypes		
Time constants (τ)	0	2	5	0	27	34
Dissociation constants (K_d) and Michaelis constants (K_m)	6	6	9	5	3	29
Enzyme turnovers (V_{max})	0	3	5	1	3	12
Initial concentrations ([])	7	7	3	1	3	21
Total	13	16	24	7	36	96

From Purkinje cells, Parameter values from measurements in cerebellar Purkinje cells; From other cells, parameter values from measurements in non-Purkinje cells, because data do not exist for Purkinje cells; From reaction in test tubes, parameter values from biochemical measurements of the reactions by purified molecules, because no data have been measured in cells; From other molecular subtypes, parameter values from biochemical measurements of purified similar subtypes, because data do not exist for the subtype measured. We used the parameter values for PLCβ1 instead of those for PLCβ4; Unknown, the remaining parameters, the values of which are not found in the literature.

based on the inhibition of Ca^{2+} release by previous incubation with Ca^{2+} (Adkins and Taylor, 1999).

We also assumed that the Ca^{2+} inactivation reactions were slower than the Ca^{2+} and IP_3 activation reactions. Because of the difference in time constants for the Ca^{2+}-dependent IP_3R activation and inactivation, IP_3Rs are transiently activated and then gradually inactivated by Ca^{2+} elevation.

Initial state in the simulation

We defined the baseline as the stable equilibrium point in the absence of any PF or CF inputs. All simulation started from the baseline. $[Ca^{2+}]_i$ and $[IP_3]$ at baseline converged at 0.06 and 0.1 μM, respectively. The baseline 0.1 μM $[IP_3]$ in our model is consistent with the 0.04 μM $[IP_3]$ measured in *Xenopus* oocytes (Luzzi et al., 1998).

Simulator and numerical integration

We ran the model on a computer by using the GENESIS simulator with Kinetikit interface (Bhalla and Iyengar, 1999). The exponential Euler method (MacGregor, 1987) with a time step of 1 μs was used to solve the differential equations.

Definition of time-window function

The time window of the Ca^{2+} response was defined as the average relative change in fluorescence ($\Delta F/F_0$) of Ca^{2+} indicator as a function of the time difference between the PF input and the CF input. The indicator is Magnesium Green 1 (250 μM; K_d = 19 μM; F_{max}/F_{min} = 2). The time difference between the PF input and the CF input is identical to the time of the CF input because we applied the PF input at 0 ms. $\Delta F/F_0$ was averaged from the first input (either PF or CF) to 500 ms after the final input of PF and CF. This time-window definition is as per the method used to analyze results of the Ca^{2+} imaging experiment (Wang et al., 2000) for direct comparisons. $\Delta F/F_0$ in the simulation is calculated by the following formula:

$$\Delta F/F_0 = \frac{[\text{MgGreen}] + [\text{MgGreen–Ca}^{2+}](F_{max}/F_{min})}{[\text{MgGreen}]_0 + [\text{MgGreen–Ca}^{2+}]_0(F_{max}/F_{min})} - 1. \quad (4)$$

The numerator and denominator are present fluorescence and basal fluorescence, respectively. MgGreen denotes free Magnesium Green 1, and MgGreen–Ca^{2+} is a binding form of MgGreen and Ca^{2+}. F_{max}/F_{min} is the ratio of the maximum fluorescence to the minimum fluorescence.

Estimation of the values of unknown parameters

The schematic model as shown in Figure 1 illustrates the molecular interactions. The interactions were described by biochemical reactions as graphically shown in supplemental Figure 1 (available at www.jneurosci.org as supplemental material). Our model consists of 53 variables and 96 parameters (supplemental Tables 1 and 2, available at www.jneurosci.org as supplemental material). To make the model as realistic as possible, the values for the parameters were estimated from experimental data obtained in cerebellar Purkinje cells, if they were available. When such data did not exist, experimental data from other cells, chemical reaction in test tubes, and other similar subtypes were used, in that order of preference (Table 1) (for more detailed information, see supplemental Table 3, available at www.jneurosci.org as supplemental material). These above parameters, the values of which were taken from the literature, are defined as known parameters. The remaining parameters are defined as unknown parameters. These values were chosen for unknown parameters so that the simulation results did not contradict the various known experimental findings, as explained in detail below.

Time constants τ, obtained from k_f and k_b, are dominant in the unknown parameters. Slow reactions in the signaling pathway often relay the signaling stimulus with delay. We assumed unreported τ values to be shorter than 10 ms to prevent them from significantly affecting the simulation results without compelling reason.

Three values of the 29 dissociation constants K_d and Michaelis constants K_m were assumed (K_d of two putative low-affinity Ca^{2+} buffers and K_m of the binding of mGluR and Gq). The two buffers were assumed to chelate free cytosolic Ca^{2+} at >10 μM $[Ca^{2+}]_i$ (Maeda et al., 1999). The K_d of nonactivated mGluR for Gq was chosen so that half of the mGluRs bound to Gq in the absence of Glu. A high K_d value tends to allow mGluRs to bind Gq before glutamate release, whereas low K_d values do not.

Three of the 12 parameter values of maximum enzyme velocities V_{max} were assumed (Gq activation by Glu-bound mGluRs, IP_3 production by Ca^{2+}-bound PLCβ without Gq, and IP_3 degradation by IP_3 3-kinase). The V_{max} of Gq activation by Glu-bound mGluRs greatly influences the peak amplitude of the IP_3 response to the PF input in the positive direction. High IP_3 peaks result in a large increase in Ca^{2+} (>10 μM) to PF input alone, whereas low IP_3 peaks result in small increases in Ca^{2+} (~2 μM), even when conjunctive PF and CF inputs are applied regardless of the time difference between the PF input and the CF input. To reproduce the supralinearity of the Ca^{2+} response to PF and CF inputs (Wang et al., 2000), the V_{max} value was chosen. We also adjusted the V_{max} value so that the PF input would produce 3 μM IP_3. The IP_3 amplitude in our model is consistent with the amplitude reported in a study of Ca^{2+} imaging and IP_3 uncaging (Finch and Augustine, 1998). The investigators in that study compared Ca^{2+} responses to photolysis of caged-IP_3 and to PF stimulation. They estimated that 16 PF stimuli at 60 Hz produce 10–20 μM IP_3 in the presence of an AMPAR antagonist. In our model, mGluR activation with 16 PF stimuli at 60 Hz evokes 10.3 μM IP_3. A balance between IP_3 production and degradation that would maintain 0.1 μM $[IP_3]$ at the baseline and reproduce the width of the time window (Wang et al., 2000) was assumed.

Of the 21 molecules in the model, concentrations of three have never been reported (SERCA, PMCA, and Na^+/Ca^{2+}). Their concentrations were chosen to reproduce their relative contributions to intracellular Ca^{2+} clearance at different $[Ca^{2+}]_i$ (Fierro et al., 1998) and to maintain the baseline $[Ca^{2+}]_i$ at 0.06 μM.

Results

Supralinear Ca^{2+} response induced by conjunctive PF–CF input in the single-spine model

We confirmed that the supralinear Ca^{2+} response to conjunctive PF and CF stimulation was reproduced in the single-spine model with the parameter set shown in supplemental Tables 1 and 2 (available at www.jneurosci.org as supplemental material). Figure 3*A* shows simulated Ca^{2+} responses when PF and/or CF inputs were applied at times 0 and 100 ms. PF input alone yielded five Ca^{2+} transients of ~1 μM (Fig. 3*A*, green, arrow 1) as a result of Ca^{2+} influx via the AMPAR pathway and a subsequent slow Ca^{2+} increase (arrow 2) because of IP_3 production via the metabotropic pathway. CF input alone evoked a sharp Ca^{2+} transient with a peak of 2 μM (Fig. 3*A*, red). The Ca^{2+} response to conjunctive PF–CF inputs (Fig. 3*A*, blue) yielded a supralinear

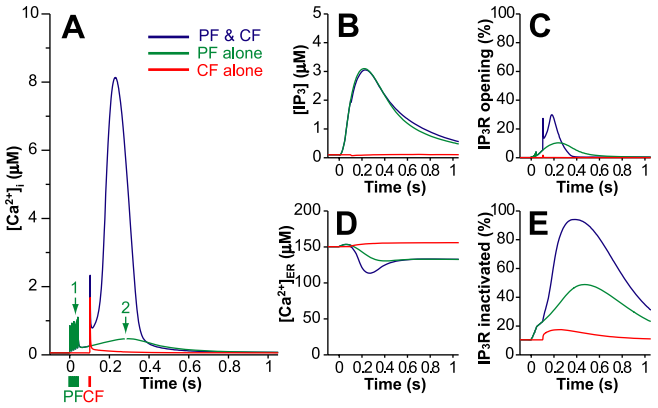

Figure 3. Time courses of simulated molecular concentrations in response to PF input (green), CF input (red), and conjunctive PF–CF inputs (blue). PF and CF inputs are applied at 0 and 100 ms, respectively. *A*, Free cytosolic Ca^{2+} concentration ($[Ca^{2+}]_i$). *B*, IP_3 concentration ($[IP_3]$). *C*, Percentage of open IP_3Rs. *D*, Free Ca^{2+} concentration in the ER ($[Ca^{2+}]_{ER}$). *E*, Percentage of inactivated IP_3Rs.

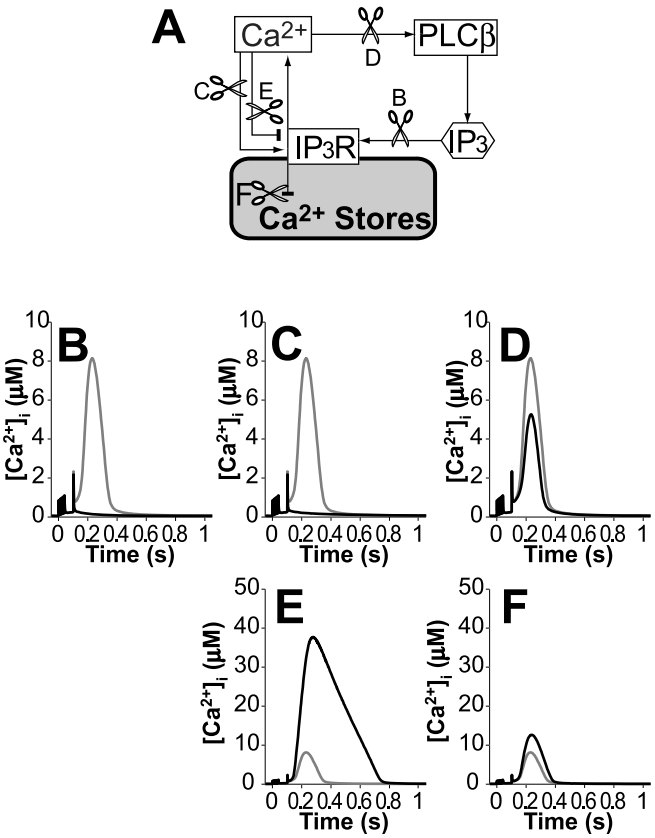

Figure 4. Pathway deletion analysis. PF and CF inputs are given at 0 and 100 ms, respectively. Pathway deletion was started at the CF input. When a pathway in which molecule A (downstream) is dependent on molecule B (upstream) in Equation 1 was deleted, the concentration of B was fixed at the baseline in Equation 2, and changes in molecules A and AB were calculated. If the upstream molecules were involved in multiple reactions (i.e., Ca^{2+}), we maintained the molecular concentration constant only in the deleted reaction, and the molecular concentrations in the other reactions varied as usual. *A*, Illustration of the specific pathways deleted in the diagrams below. *B–F*, The black and gray lines indicate time course of $[Ca^{2+}]_i$ in the deleted pathway and under control conditions (identical to Fig. 3*A*, blue), respectively. *B*, Deletion of the IP_3-dependent IP_3R activation pathway. *C*, Deletion of the $[Ca^{2+}]_i$-dependent IP_3R activation pathway. *D*, Deletion of the $[Ca^{2+}]_i$-dependent PLCβ activation pathway. *E*, Deletion of the $[Ca^{2+}]_i$-dependent IP_3R inactivation pathway. *F*, $[Ca^{2+}]_{ER}$ is held constant at the baseline concentration.

signal (8.1 μM peak at 230 ms), and it returned to the basal level within 1 s. The supralinearity of the simulated Ca^{2+} responses is similar to the supralinearity observed in the Ca^{2+} imaging experiment (Wang et al., 2000), but not exactly the same. At <1 μM $[Ca^{2+}]_i$, the increase in fluorescence ($\Delta F/F_0$) is approximately proportional to the increase in $[Ca^{2+}]_i$, and the ratio is 0.2 μM $\Delta[Ca^{2+}]_i$ per percentage of $\Delta F/F_0$.

Cytosolic IP_3 gradually accumulated after the PF inputs (3.1 μM peak at 220 ms) (Fig. 3*B*, green), and the CF input had little influence on the IP_3 dynamics (Fig. 3*B*, compare blue, green). The proportion of open IP_3Rs in response to conjunctive PF–CF inputs reached 30% (Fig. 3*C*, blue) as opposed to only 10% in response to PF input alone (Fig. 3*C*, green) and 1.7% in response to CF input alone (Fig. 3*C*, red). Therefore, CF-mediated Ca^{2+} transients triggered IP_3R activation only during IP_3 elevations. The supralinear Ca^{2+} response was induced by Ca^{2+} release from the ER Ca^{2+} stores as a result of opening IP_3Rs, as indicated by the increase in open IP_3Rs (Fig. 3*C*, blue) and the reduced Ca^{2+} concentration in the ER (Fig. 3*D*, blue). More than 90% of the IP_3Rs were in the inactivated state after the conjunctive PF–CF input (Fig. 3*E*, blue), indicating that IP_3R inactivation terminated the supralinear Ca^{2+} signal.

Ca^{2+}-dependent IP_3R activation and inactivation are essential for supralinear Ca^{2+} dynamics

Supralinear Ca^{2+} dynamics may be mediated by a positive feedback loop(s) in the signaling pathways. We identified two candidate positive feedback loops for the supralinear Ca^{2+} signal in the block diagram (Fig. 1). One is the Ca^{2+}-dependent IP_3R activation loop. Ca^{2+} elevation may open IP_3Rs, resulting in additional Ca^{2+} elevation ($Ca^{2+} \rightarrow IP_3Rs \rightarrow Ca^{2+}$). The other is the loop of Ca^{2+}-dependent IP_3 production by PLCβ. Ca^{2+} elevation may enhance the activity of PLCβ for IP_3 production, and IP_3 elevation may open IP_3Rs and release Ca^{2+} from the ER, resulting in additional Ca^{2+} elevation ($Ca^{2+} \rightarrow PLC\beta \rightarrow IP_3 \rightarrow IP_3Rs \rightarrow Ca^{2+}$). The diagram also contains two negative feedback loops for terminating Ca^{2+} release. The Ca^{2+}-dependent IP_3R inactivation loop may inhibit IP_3R opening at high Ca^{2+} concentration. Alternatively, Ca^{2+} release may continue until depletion of the Ca^{2+} in the ER stores.

We deleted reactions to identify the dominant pathways responsible for Ca^{2+} dynamics (Fig. 4*A*), by maintaining the molecular concentration on the upstream side of the reaction constant at its basal concentration. For example, when the IP_3-dependent IP_3R activation reaction is deleted (Fig. 4*B*), the IP_3Rs are exposed to IP_3 at the basal concentration, whereas the IP_3-dependent reactions (degradation by IP_3 3-kinase and 5-phosphatase) react with variable IP_3 concentration.

The first reaction we deleted was IP_3 binding to IP_3Rs. We prevented IP_3R activation from increasing IP_3. There was no supralinear Ca^{2+} response at all (Fig. 4*B*), indicating that supralinear Ca^{2+} signals require IP_3 elevation. When IP_3R activation was deleted by fixing the Ca^{2+} concentration for the IP_3R activation alone, the supralinear Ca^{2+} response was completely eliminated (Fig. 4*C*), whereas deletion of the pathway of PLCβ activation by Ca^{2+} did not eliminate the supralinear Ca^{2+} response (Fig. 4*D*). These results indicate that the supralinear Ca^{2+} response to conjunctive PF-CF inputs is a regenerative process driven by the positive feedback loop in which Ca^{2+} induces Ca^{2+} release through the IP_3Rs.

Deletion of the IP_3R inactivation reaction dramatically prolonged and increased the $[Ca^{2+}]_i$ elevation (Fig. 4*E*). Finally, we clamped $[Ca^{2+}]$ in the ER ($[Ca^{2+}]_{ER}$) at 150 μM, the basal con-

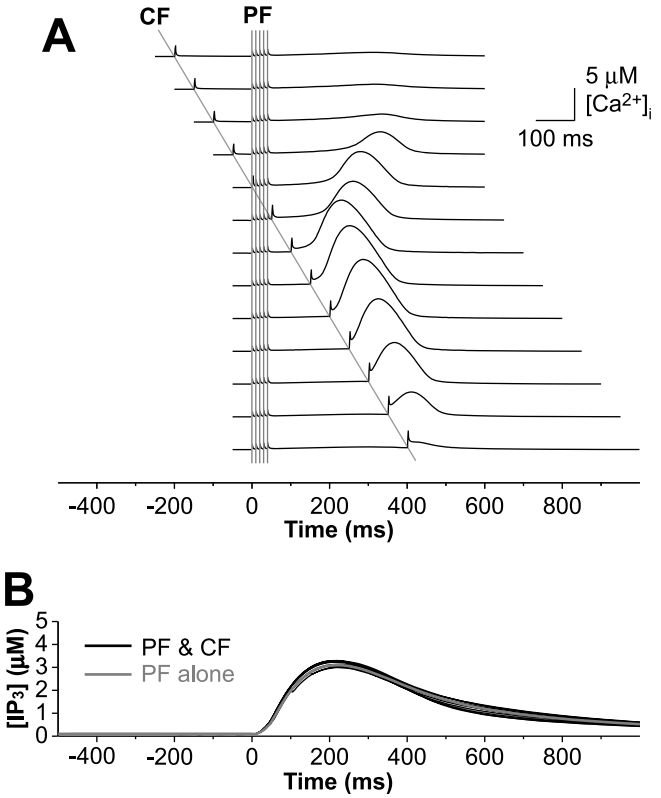

Figure 5. Regenerative Ca^{2+} release dependence on the timing of PF–CF inputs. *A*, Ca^{2+} responses to conjunctive PF–CF inputs with various intervals between the PF input and CF input. The PF input is delivered at 0 ms, indicated by the five repetitive lines. CF input is delivered at −200 to + 400 ms, as indicated by the single line. *B*, Overplot of IP_3 time courses in response to the various PF–CF inputs.

centration. By maintaining the $[Ca^{2+}]_{ER}$ constant, we prevented the gain and loss of $[Ca^{2+}]_{ER}$ attributable to Ca^{2+} release through the IP_3Rs, Ca^{2+} uptake by Ca^{2+} pumps, and so on. The constant $[Ca^{2+}]_{ER}$ did not significantly alter the time course of changes in $[Ca^{2+}]_i$ (Fig. 4*F*). Thus, Ca^{2+}-dependent IP_3R inactivation, not Ca^{2+} depletion in the ER, is essential and solely responsible for terminating the Ca^{2+}-induced Ca^{2+} release.

PF–CF time window of the Ca^{2+} response is controlled by the changes in IP_3 concentration over time

To explore the molecular mechanisms responsible for the detection of spike timing, conjunctive PF–CF inputs were applied at various intervals between the PF input and the CF input, as shown in Figure 5*A*. The Ca^{2+} response reached at least 5 μM when the CF input followed PF input within intervals of 0–300 ms (Fig. 5*A*). Application of PF–CF inputs in the reverse order did not evoke regenerative Ca^{2+} release. The time course of IP_3 concentrations did not change much at different PF–CF intervals, and it was always time-locked to the PF input (Fig. 5*B*).

To evaluate the timing-dependent Ca^{2+} responses as a function of the PF–CF time interval quantitatively, the time-window function of the Ca^{2+} response was defined as the time-integrated $\Delta F/F_0$ from the first input to 500 ms after the last input (compare Fig. 6*A*) (see Materials and Methods), as per the method used to analyze results of Ca^{2+} imaging (Wang et al., 2000). The time-window function is plotted as a solid curve in Figure 6*B*.

The time-window function was large between 0 and 300 ms, and Gaussian fitting to the time window yielded a peak time of 114 ms and half-width of 170 ms, consistent with the results of the

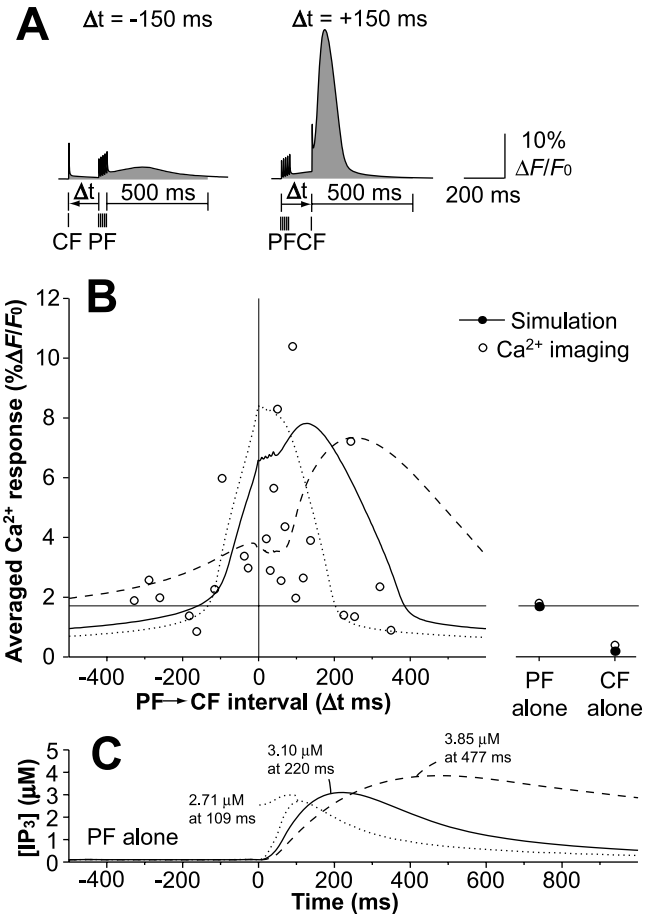

Figure 6. Time window of the Ca^{2+} response controlled by the IP_3 time course. *A*, Examples of the time-integral interval of the Ca^{2+} response to PF–CF inputs. The PF–CF interval, Δt, is defined as the time between the start of the PF input to the start of the CF input. Ca^{2+} response is defined as the average increase in fluorescence ($\Delta F/F_0$) from the first stimulus to 500 ms after the final stimulus. The Ca^{2+} indicator is Magnesium Green 1 ($K_d = 19$ μM; $F_{max}/F_{min} = 2$). *B*, Time window of Ca^{2+} response as a function of the PF–CF interval, controlled by the IP_3 time course. Ca^{2+} responses to the PF or CF input alone in the simulation and the Ca^{2+} imaging results are plotted on the right as closed and open circles, respectively. The simulated time window (solid line) is compared with the Ca^{2+} imaging data (open circles) (Wang et al., 2000). The dotted and broken lines indicate time windows when IP_3 peak time (*C*) in response to the PF input alone was shifted to earlier and to later times by modifying enzymatic parameters.

Ca^{2+} imaging experiments (peak time, 92 ms; half-width, 212 ms) (Wang et al., 2000). A very similar time window was obtained when we used $[Ca^{2+}]_i$ instead of $\Delta F/F_0$ as a measure of the Ca^{2+} response (data not shown). Thus, it can be concluded that the supralinear Ca^{2+} response is not attributable to a saturating effect of the fluorescent indicator. Ca^{2+} influx attributable to PF and CF activation outside the above effective time window did not trigger major Ca^{2+} release from the ER.

Temporal similarity was found between the slow IP_3 response and the time-window function (Fig. 6*B*,*C*, compare solid curves), suggesting that the IP_3 time course accounts for spike-timing detection. To systematically verify that the IP_3 time course actually does determine the time window of the Ca^{2+} response, we intentionally manipulated the IP_3 time course by varying two-parameter values in the model as described below and then plotted the time windows. The GTPase activation protein (GAP) activity of PLCβ promotes Gq inactivation, and the maximum enzyme velocity of GAP was increased fivefold to shift the IP_3 peak time to an earlier time. At the same time, the maximum

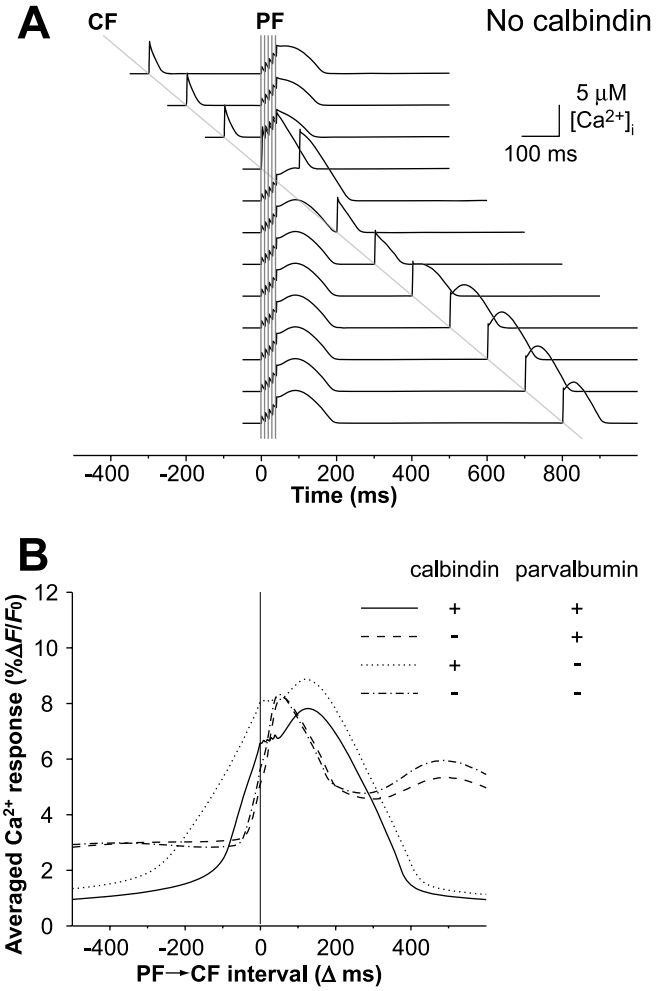

Figure 7. Ca^{2+} buffers contribute to shaping the time window of Ca^{2+} response. *A*, Ca^{2+} responses to conjunctive PF–CF inputs with various timings, identical to Figure 5*A*, except for in the absence of the high-affinity Ca^{2+} buffer calbindin. *B*, The time window of the Ca^{2+} response without calbindin and/or paravalbumin.

velocity of enzyme catalysis of IP_3 production by PLCβ with Ca^{2+} and Gq was increased 3.5-fold to maintain the peak amplitude of the time window of Ca^{2+} responses. As a result, the time window narrowed and shifted to an earlier time (Fig. 6*B*,*C*, dotted lines). To shift the IP_3 peak to a later time, on the other hand, the maximum enzyme velocities of GAP and IP_3 production were decreased 0.2- and 0.5-fold, respectively, and as a result, the time window expanded and shifted to a later time (Fig. 6*B*,*C*, broken lines). Thus, the time-window function of the Ca^{2+} response depended on the IP_3 time course.

Cerebellar Purkinje cells contain high concentrations of high-affinity buffers, such as calbindin and parvalbumin (Fierro and Llano, 1996; Maeda et al., 1999). These buffers hinder increases in $[Ca^{2+}]_i$ at <1 μM $[Ca^{2+}]_i$ but saturate at >1 μM $[Ca^{2+}]_i$. We explored the effect of eliminating the high-affinity buffers on the time window of the Ca^{2+} response. In the absence of calbindin, PF or CF input produces a large Ca^{2+} increase to $\sim$5 μM (Fig. 7*A*). The time window of the Ca^{2+} response had two peaks, a time difference between the PF and CF inputs of one $\sim$0 ms and the other $\sim$500 ms (Fig. 7*B*). The first peak indicates that calbindin prevents only the Ca^{2+} influx in response to conjunctive PF–CF inputs from producing a regenerative increase in Ca^{2+}. The second peak appeared because the IP_3 elevation persisted and the inactivation of IP_3R recovered at 500 ms. Elimination of parvalbumin, the other high-affinity buffer in the simulation, did not have any significant effect on the Ca^{2+} responses (Fig. 7*B*). We therefore concluded that calbindin is essential for timing detection.

Regenerative Ca^{2+} release as a threshold phenomenon regulated by $[IP_3]$

Qualitatively different Ca^{2+} dynamics at different IP_3 levels were systematically analyzed and visualized while simplifying the simulated PF input as a step-function elevation in IP_3 (Fig. 8*A*), because the IP_3 response to the PF input is much slower than the Ca^{2+} response (Fig. 5*B*). We analyzed Ca^{2+} changes in response to three different constant IP_3 levels: 0.1 μM (actually no change), 2.5 μM, and 10 μM (Fig. 8*A*). The first IP_3 level, 0.1 μM, is identical to the baseline condition. The second IP_3 level, 2.5 μM, corresponds to the IP_3 concentration 100 ms after the PF input (Fig. 3*B*), and the third level, 10 μM, is excessively high and was obtained by IP_3 uncaging (Khodakhah and Ogden, 1995; Finch and Augustine, 1998). From the baseline concentration of 0.1 μM, $[IP_3]$ was changed to one of the three levels in a step function and held constant (Fig. 8*A*). Synchronized with this IP_3 step-up, an influx of a different amount of Ca^{2+} was delivered for 2 ms (Fig. 8*B*), the same duration as the simulated CF input. The time courses of $[Ca^{2+}]_i$ and IP_3R inactivation are shown in Figure 8, *C* and *D*, respectively, and they are also plotted as trajectories on phase planes in Figure 8*E*. The different amounts of Ca^{2+} influx are color-coded in Figure 8*B*, and their responses are correspondingly color-coded in Figure 8*C–E*.

At 0.1 μM IP_3, $[Ca^{2+}]_i$ monotonically decreased after the Ca^{2+} influx (Fig. 8*C*,*E*, left), and larger Ca^{2+} influxes produced higher Ca^{2+} peaks and stronger IP_3R inactivation (Fig. 8*C*,*D*, left). The trajectories were evenly distributed spatially in the phase plane (Fig. 8*E*, left), indicating almost linear responses to Ca^{2+} influx.

At 2.5 μM IP_3, $[Ca^{2+}]_i$ monotonically decreased after the influx when the Ca^{2+} transients at the end of the Ca^{2+} influx were $\leq$2 μM, whereas when they were larger than 3 μM, $[Ca^{2+}]_i$ dropped very briefly and then increased back to $>$10 μM (Fig. 8*C*, middle inset). Thus, Ca^{2+} dynamics can be classified into suprathreshold responses and subthreshold responses bounded by a threshold of 2–3 μM Ca^{2+} transient. The trajectories around this threshold were very sparsely spaced (Fig. 8*E*, middle, compare the light and dark blue trajectories), which also confirms the nonlinear threshold phenomenon.

At 10 μM IP_3, $[Ca^{2+}]_i$ increased to $>$15 μM without any Ca^{2+} influx (Fig. 8*C*, right, black line), indicating that the baseline $[Ca^{2+}]_i$ was already high enough to induce regenerative Ca^{2+} release in the presence of high IP_3. There was a latency of 50 ms in the Ca^{2+} response in the absence of a Ca^{2+} influx (Fig. 8*C*, right, black line), indicating that the positive feedback loop of regenerative Ca^{2+} release requires a relatively long build-up time to be fully activated at low $[Ca^{2+}]_i$. A larger Ca^{2+} influx elevated the $[Ca^{2+}]_i$ peak and reduced this latency (Fig. 8*C*, right, compare the latency of different lines), which is consistent with the IP_3-induced Ca^{2+} increase in experimental studies (Khodakhah and Ogden, 1995; Finch and Augustine, 1998).

Figure 8*F* is a color-coded contour map of the averaged Ca^{2+} response over 500 ms as a function of the transient Ca^{2+} peaks (see initial peaks in Fig. 8*C*, middle inset) along the ordinate and the constant IP_3 level along the abscissa. First, the averaged Ca^{2+} response increased with the size of the transient Ca^{2+} peak and the concentration of IP_3. However, the Ca^{2+} dynamics were

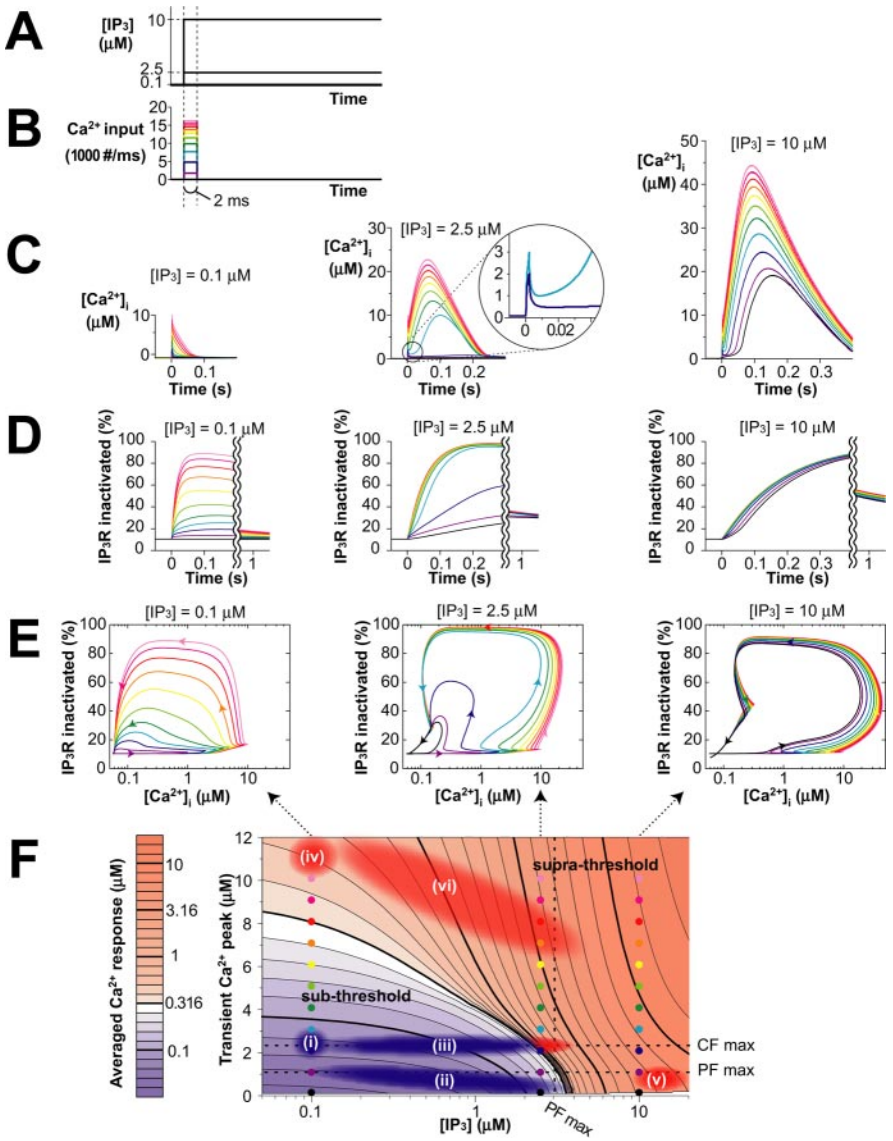

Figure 8. Ca^{2+} dynamics with threshold dependent on $[IP_3]$. *A*, $[IP_3]$ was step-changed to 0.1, 2.5, or 10 μM from the steady state, 0.1 μM, at time 0 ms. *B*, The 2 ms Ca^{2+} influx started to be delivered at the same time, 0 ms. The amounts of Ca^{2+} influx were adjusted so that the transient Ca^{2+} peaks for 2 ms were 1 μM (violet), 2 μM (dark blue), 3 μM (light blue), 4 μM (dark green), 5 μM (light green), 6 μM (yellow), 7 μM (orange), 8 μM (red), 9 μM (magenta), and 10 μM (pink). The black lines indicate that no Ca^{2+} influx was delivered. *C*, Response of $[Ca^{2+}]_i$ to the combination of step-changed $[IP_3]$ and Ca^{2+} influx. Inset, Enlargement of the $[Ca^{2+}]_i$ response, the transient Ca^{2+} peaks of which were 2 and 3 μM at 2.5 μM $[IP_3]$. *D*, Response of IP_3R inactivation rate to the combination of step-changed $[IP_3]$ and Ca^{2+} influx. *E*, Trajectories in *C* (*t-x* plane) and *D* (*t-y* plane) were mapped on the phase plane of $[Ca^{2+}]_i$ versus the IP_3R inactivation rate (*x-y* plane). Arrows indicate the time directions in the trajectories. *F*, Average Ca^{2+} response over 500 ms after inputs is colored in the contour map as a function of step-changed $[IP_3]$ and the transient Ca^{2+} peak. The bar at the left illustrates the color and contour scales of the averaged Ca^{2+} response. The red area indicates suprathreshold responses, and the blue area indicates subthreshold responses. The three dotted lines approximately indicate the maximum levels of the transient Ca^{2+} peaks in response to CF and PF stimulation and the IP_3 amplitude in response to PF stimulation. See Discussion for the meaning of regions (i)–(vi).

qualitatively different for small, medium, and large IP_3, as already described in Figure 8*A–E*. At 0.1 μM IP_3, the contour lines were nearly horizontal, indicating that the average Ca^{2+} response was mainly determined by the amount of Ca^{2+} influx. At 10 μM IP_3, the contour lines were nearly vertical, indicating that the average Ca^{2+} response was mainly determined by the IP_3 level. The contour lines have negative diagonal slopes only in the 1–4 μM IP_3 region, indicating that both the Ca^{2+} influx and $[IP_3]$ significantly influence the average Ca^{2+} response. Moreover, the contour lines were densely packed in this region alone, indicating the threshold for a large Ca^{2+} release.

Robustness of the response of the spike-timing detection mechanism to values of unknown parameters

The dependence of the supralinear Ca^{2+} response on the timing of PF–CF inputs is attributable to the delay between the PF input and the IP_3 peak (Fig. 6*B*,*C*). We explored the relationships between the robustness of the IP_3 time course in response to the PF input alone and against variations in each of the parameter values. The value for each parameter was varied from 1/100- to 100-fold the standard value with the value for all other parameters constant. The results of the sensitivity analysis of the IP_3 time course in relation to each parameter are shown in supplemental Figure 2*A–E* (available at www.jneurosci.org as supplemental material). Although the IP_3 time course was robust to the variations in the values of most of the parameters, the IP_3 peak time was greatly affected by some parameters for maximum enzyme velocities (V_{max}): Gq activation by Glu–mGluR (parameter ID in supplemental material: a5; available at www.jneurosci.org), IP_3 production by PLCβ without Gq (b6) and with Gq (b7), GAP activity of PLCβ (b10, b11, b12), and IP_3 degradation by IP_3 3-kinase (c3). The values of only three of these critical parameters (a5, b6, and c3) were unknown. Parameter a5 was chosen so that the mGluR pathway produces 10 μM IP_3 at 16 PF pulses, based on Ca^{2+} response to uncaging IP_3 (Finch and Augustine, 1998). Parameters b6 and c3 were chosen to maintain the basal $[IP_3]$ level at 0.1 μM. Figure 9 shows time courses of IP_3 concentrations in relation to differences in the values (1/10- to 10-fold) of the three unknown parameters. Gq activation by Glu–mGluR (a5) had a major effect on the height of the peak of IP_3 concentration but not on the time of the peak (Fig. 9*A*). When we applied large V_{max} (10-fold the control) of IP_3 production by PLCβ in the absence of Gq (b6), we obtained a prolonged IP_3 response (Fig. 9*B*). IP_3 degradation by IP_3 3-kinase (c3) affected both the peak amplitude and the time of the peak (Fig. 9*C*). A larger V_{max} of IP_3 degradation by IP_3 3-kinase decreased the peak amplitude and shifted the peak to an earlier time.

Next, we examined the robustness of the time window of PF–CF inputs and the time course of the concentration of the changes in IP_3. Each parameter was varied from 1/100- to 100-fold of its standard value with all other parameters constant, and the behavior of the model was quantified in terms of the peak time, half-width, and peak amplitude of the temporal window

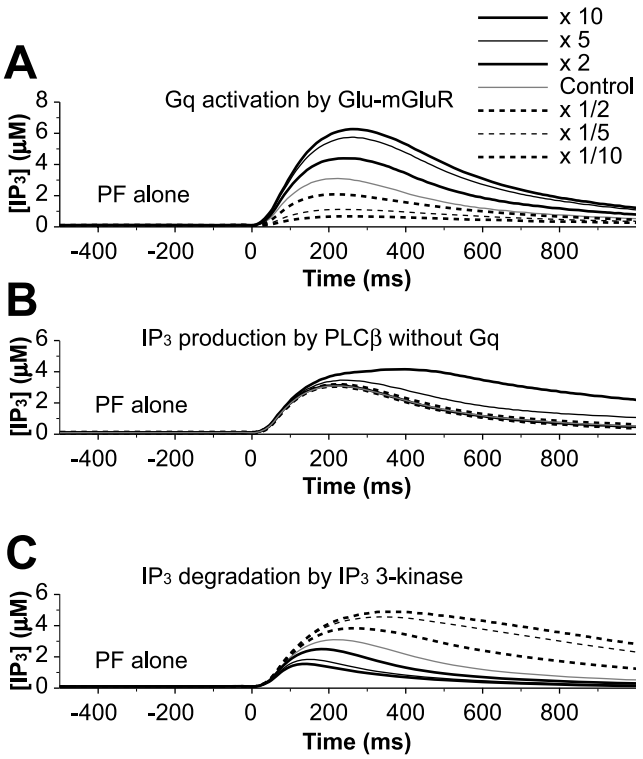

Figure 9. Sensitivity of the IP_3 time course to variations in parameter values. Three unknown maximum enzyme velocities that affect the IP_3 time course are shown as representative examples. The parameters were varied within the 1/10- to 10-fold range. *A*, Gq activation by Glu–mGluR complex. *B*, IP_3 production by PLCβ without Gq. *C*, IP_3 degradation by IP_3 3-kinase.

after Gaussian fitting (supplemental Fig. 2*F*,*G*; available at www.jneurosci.org as supplemental material). The results of the sensitivity analysis of the time window for each parameter are shown in supplemental Figure 2*H–K* (available at www.jneurosci.org as supplemental material). The parameters in the model were classified into four categories: time constants, dissociation and Michaelis constants, maximum enzyme velocities, and initial concentrations. Figure 10 shows graphs of the average changes and SDs of the peak time (left column), half-width (middle column), and peak amplitude (right column) when the values were varied as indicated along the abscissa of these four classes of parameters. Similar tendencies were shown between parameters with values that are known (black) and unknown (gray). The three characteristics of the temporal window changed little in response to small differences in the parameters (one-half or two times). Most importantly, even major changes in parameters (1/100–100 times) had little effect on the peak time and half-width, although peak amplitudes sometimes changed considerably. Because spike-timing detection is essentially characterized by the shape of the temporal window (i.e., the peak time and half-width), we concluded that the proposed model is very robust in its most important characteristic (i.e., spike-timing detection for a large range of parameter variations).

Discussion

Because many signal transduction pathways interact with each other and often exhibit nonlinear dynamics, it would be difficult to understand complex cellular information processing on the basis of experiments alone. Computational kinetic simulation may make it possible to determine whether known signaling pathways are sufficient to reproduce cellular events of interest and make it possible to fully understand the mechanisms of the information processing performed by the molecular dynamic networks. In this study, we modeled Ca^{2+} dynamics within a single spine to elucidate the actual mechanism of spike-timing detection. Supralinear Ca^{2+} responses were generated by Ca^{2+}-dependent IP_3R activation during IP_3 elevation, and the PF–CF time window was determined from the time course of changes in IP_3 concentrations. PF-mediated IP_3 elevation lowered the Ca^{2+} threshold, and CF-mediated Ca^{2+} influx triggered Ca^{2+} release through the IP_3Rs. Three Ca^{2+} responses exhibit different dynamics at low, medium, and high IP_3 concentrations.

IP_3 regulation of Ca^{2+}-induced Ca^{2+} release and the PF–CF time window

In Figure 11*A*, the IP_3-dependent Ca^{2+} threshold indicates the Ca^{2+} input required for IP_3 concentration at the time, so that averaged Ca^{2+} response in the 500 ms after the CF input is >3.16 μM (Fig. 8*F*, bold line between the blue area and red area), dependent on IP_3 at this time (Fig. 5*B*). The Ca^{2+} threshold represents the size of the Ca^{2+} increase required for a large Ca^{2+} response, if the CF input is applied at the time. The IP_3-dependent Ca^{2+} threshold explains the optimal timing of the PF input for the regenerative Ca^{2+} response. CF input within 300 ms after PF input induces a Ca^{2+} transient and causes the Ca^{2+} response to reach the threshold (Fig. 11*A*, black line). In contrast, when the CF input occurs before the PF input (Fig. 11*A*, thick gray line) or occurs too late after the PF input (Fig. 11*A*, dotted gray line), the CF-mediated Ca^{2+} influx does not increase Ca^{2+} concentrations enough to reach the threshold.

Regenerative Ca^{2+}-induced Ca^{2+} release via IP_3Rs accounts for the supralinear Ca^{2+} signals. First, Ca^{2+}-induced Ca^{2+} release was initiated by CF-mediated Ca^{2+} entry in the presence of increased IP_3, then accelerated by the positive feedback loop of Ca^{2+}-dependent IP_3R activation, and finally terminated by the negative feedback loop of Ca^{2+}-dependent IP_3R inactivation (Fig. 11*B*).

The results of the sensitivity analysis (Figs. 9, 10) (supplemental Fig. 2, available at www.jneurosci.org as supplemental material) reliably support the notion that the spike-timing detection mechanism is not dependent on parameter values but on the model structure, specifically on the difference in time scale between a rapid electrical reaction (Ca^{2+} influx by depolarization) and a slow biochemical reaction (IP_3 production by the metabotropic pathway). However, it should be pointed out that although the results of our simulation support our hypothesis, they do not exclude possibilities of other functions of the pathways or additional pathways.

The temporal relationship between the coincidence of the PF and CF inputs must be detected at some point of intersection between the two signal transduction pathways downstream to the PF and CF inputs, because we found only one possible intersection point in the MAP kinase cascade in addition to the IP_3Rs cascade in an LTD signaling model we previously proposed (Kuroda et al., 2001). CF input stimulates the MAP kinase cascade, whereas PF input activates the nitric oxide (NO)/cGMP pathway, which plays a gating role in allowing activation of the MAP kinase cascade. However, because activation of the NO/cGMP pathway is too slow (order of minutes) to detect subsecond timing (Hartell et al., 2001), IP_3Rs and the upstream pathways must detect the timing of the PF and CF inputs. Wang et al. (2000) have proposed that IP_3Rs themselves may detect the temporal order of the changes in IP_3 and Ca^{2+}. IP_3Rs may be inactivated by the CF-mediated Ca^{2+} influx before the PF-mediated IP_3 elevation, be-

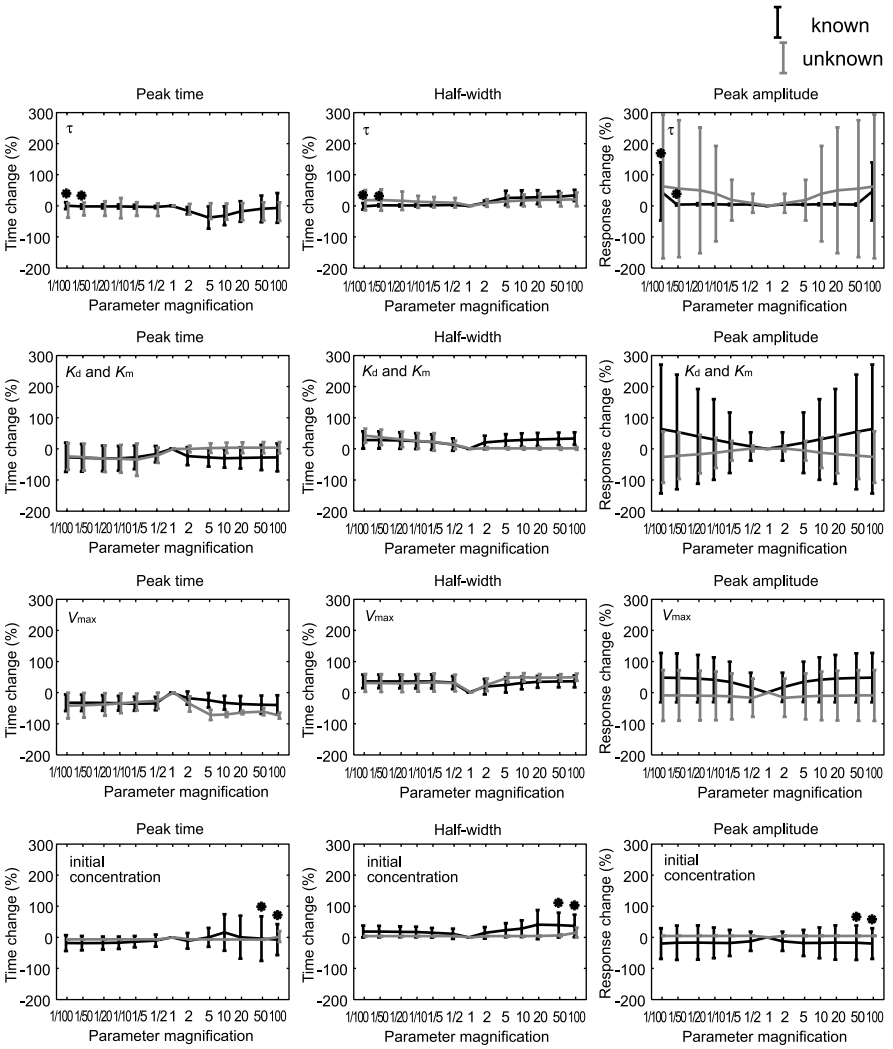

Figure 10. Percentage of changes in the three characteristic quantities of the time window induced by changes in parameter values. All parameters were classified as time constants (first row), dissociation and Michaelis constants (second row), maximum enzyme velocities (third row), and initial concentrations (fourth row). Each parameter was varied within a range of 1/100- to 100-fold with other parameters maintained constant. The time window was simulated for this set of parameters and was fitted by a Gaussian function. The percentage of changes in the peak time (left), half-width (middle), and peak amplitude (right) of the Gaussian function compared with those of the original time window in Figure 6*B* were computed and then averaged over parameters within the four categories. These averaged changes in the characteristic quantities were plotted as a function of the magnification (minification) factor of the changed parameter. The known and unknown parameters are marked in black and gray, respectively. The bars represent ±SD. The asterisks in some figures mean that one or two of the computations could not be completed because of numerical explosions.

cause IP_3-evoked Ca^{2+} release is inhibited by preincubation with Ca^{2+} (Khodakhah and Ogden, 1995; Adkins and Taylor, 1999) and thus can only be activated by the PF–CF order. However, the Ca^{2+} response to the CF input was much weaker in our simulation (Fig. 3*A*, red) than the strong Ca^{2+} stimulation in their experiments (10 or 100 μM for ~1 s). Thus, this first possibility is unlikely to account for the detection of the timing. Instead, the kinetics of IP_3 binding to IP_3Rs may be slow and result in the necessary time difference, and this seemed to be experimentally supported by a latency of ~50 ms in IP_3-evoked Ca^{2+} release (Khodakhah and Ogden, 1995; Marchant and Taylor, 1997). However, a similar latency was obtained in our simulation (Fig. 8*C*, right, black) with the fast IP_3 binding in our IP_3R kinetic model, and thus these experimental data cannot discriminate between the two mechanisms of detecting the timing.

Clear discrimination between the two possibilities is possible by measurement of the Ca^{2+} response to flash photolysis of caged IP_3 and caged Ca^{2+}. The caged compounds have different optimal wavelengths for uncaging that enable the concentrations of IP_3 and Ca^{2+} to be controlled independently. We predict that IP_3 uncaging will yield a delayed Ca^{2+} increase (Fig. 8*C*, right, black), whereas Ca^{2+} uncaging will yield an immediate and transient Ca^{2+} increase (Fig. 8*C*, left). Conjunctive Ca^{2+}–IP_3 uncaging should induce a supralinear Ca^{2+} response that is larger than the sum of the response to uncaging of Ca^{2+} alone and uncaging of IP_3 alone. The largest Ca^{2+} response would be expected in coincidental IP_3–Ca^{2+} conjunctive uncaging, unlike conjunctive PF–CF stimulation, because, unlike the metabotropic pathway, IP_3 uncaging elevates $[IP_3]$ without any delay. If delayed Ca^{2+} photolysis after IP_3 photolysis is found to be optimal, our model will be refuted.

Various LTD forms unified within a single model of Ca^{2+} dynamics

We previously modeled the signaling pathways involved in LTD induction, including the NO/cGMP pathway, MAP kinase cascade, protein kinase C activation, and AMPAR phosphorylation, which were not incorporated in the current study, and found that a supralinear Ca^{2+} increase induced by conjunctive PF and CF inputs is required for induction of LTD (Kuroda et al., 2001). However, the Ca^{2+} increase in the previous model was based on experimental observations (Wang et al., 2000) and was not modeled in a kinetic simulation. Thus, the previous and current models complement each other and could be regarded as downstream and upstream models of the entire LTD signaling transduction. The previous downstream model (Kuroda et al., 2001) computed AMPAR phosphorylation dependent on Ca^{2+} increase as one of the major inputs, whereas the current upstream model reproduced the Ca^{2+} increase with PF and CF inputs. Therefore, although we only modeled the Ca^{2+} dynamics in this study, the current model is useful for elucidating the critical role of Ca^{2+} dynamics in different forms of LTD as described below.

The various Ca^{2+} dynamics dependent on IP_3 are capable of coherently explaining various forms of LTD. We conceptually illustrated six regions of different dynamics in Figure 8*F*. First, region (i) at the baseline IP_3 shows that CF input alone yields a small Ca^{2+} transient (~2 μM $[Ca^{2+}]_i$) that does not enable the averaged Ca^{2+} response to reach the Ca^{2+} threshold. Region (i) also shows that LTD is eliminated when IP_3 production via the metabotropic pathway is inhibited. Mice lacking mGluR1 exhibit impaired LTD induction and motor learning (Aiba et al., 1994; Conquet et al., 1994). Second, region (ii) illustrates that PF input alone yields a Ca^{2+} influx of ~1 μM and a subsequent IP_3 in-

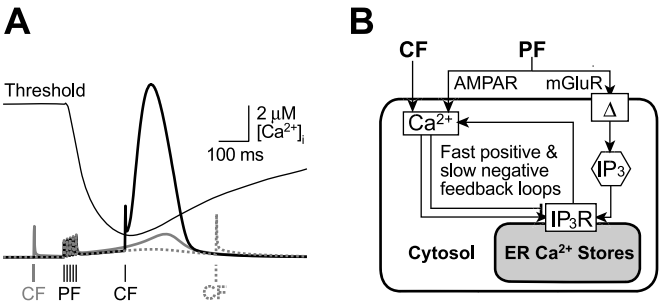

Figure 11. Schematic model of PF–CF timing detection based on changes in the Ca^{2+} threshold over time. *A*, Ca^{2+} time courses with PF–CF input intervals of −100 ms (thick gray line), +200 ms (black line), and +500 ms (dotted gray line). The threshold indicates the averaged Ca^{2+} response of 3.16 μM (Fig. 8*F*) and was computed from the IP_3 time course with the PF input alone (Fig. 3*B*, green). If the transient Ca^{2+} response to the CF input exceeds the Ca^{2+} threshold, regenerative Ca^{2+} release is triggered, and a supralinear Ca^{2+} response appears. *B*, The Δ in the mGluR pathway indicates a time delay between PF input and IP_3 accumulation. Ca^{2+} release is both activated and inactivated by the Ca^{2+} increase. In the presence of sufficient IP_3, Ca^{2+} influx triggers regenerative Ca^{2+} release by the fast positive feedback loop of Ca^{2+}-dependent IP_3R activation. After the Ca^{2+} increase, the slow negative feedback loop terminates Ca^{2+} release.

crease. The elongated region (ii) represents the transition of Ca^{2+} dynamics after PF input, starting at the left side. As IP_3 is increased by the PF input, the Ca^{2+} dynamics move to the right portion of region (ii). Ultimately, the Ca^{2+} dynamics in region (ii) never reach the threshold. Third, the horizontal region (iii) illustrates the dependency of Ca^{2+} dynamics on the timing of conjunctive PF–CF inputs. IP_3 maximally increased to 3 μM and then decreased to the baseline after PF input (Fig. 3*B*). Region (iii) represents these different IP_3 at different times with respect to the PF input, whereas the CF input induces a transient Ca^{2+} peak at the same level (Fig. 5*A*). If the CF input is applied during IP_3 elevation [dynamics jump from the right side of region (ii) to the red part of region (iii)], as when there is a delay of 0–300 ms in Figure 5*A*, the transient Ca^{2+} peak crosses the threshold and induces LTD. If the CF input and IP_3 elevation do not coincide, the transient Ca^{2+} peaks are insufficient to reach the threshold [dynamics jump from the left of region (ii) to the blue part of region (iii)]. Thus, conjunctive PF–CF inputs can induce LTD only within the appropriate time window where PF-induced IP_3 elevation provides a low Ca^{2+} threshold. Fourth, region (iv) shows that LTD induction can be induced only by application of a large Ca^{2+} elevation in the spine, even without IP_3 elevation. This is consistent with the observation that repetitive Ca^{2+} uncaging rescues the induction of LTD in Purkinje cells, the dendritic spines of which lack Ca^{2+} stores (Miyata et al., 2000). Fifth, region (v) may explain the finding that IP_3 uncaging induces Ca^{2+} release and LTD without CF activation or depolarization (Khodakhah and Ogden, 1995; Finch and Augustine, 1998). Sixth, and finally, region (vi) indicates that massive PF-bundle stimulation is capable of providing large Ca^{2+} transients that induce LTD without CF input (Hartell, 1996; Wang et al., 2000). Although IP_3 elevation contributes the Ca^{2+} transients, the Ca^{2+} influx is large enough to allow the Ca^{2+} response to reach the threshold.

The Ca^{2+} dynamics model and cerebellar learning theories

As stated in Introduction, according to cerebellar learning theories (Ito, 1970; Kawato, 1999; Yamamoto et al., 2002), LTD must be induced when PF inputs precede CF inputs. Different groups have used many different experimental paradigms and have reported a variety of time windows for LTD induction (Ekerot and Kano, 1989; Karachot et al., 1994; Chen and Thompson, 1995; Yamamoto et al., 2002). Furthermore, cerebellar motor learning theories cannot easily explain the fact that LTD induction does not necessarily require CF inputs. The IP_3-dependent Ca^{2+} threshold suggests that strong PF input alone triggers regenerative Ca^{2+} release [Fig. 8*F*, region (vi)]. LTD has been experimentally induced by strong PF activation without CF activation (Hartell, 1996), but this type of LTD apparently does not occur in natural response to stimuli or contribute to cerebellar learning. However, De Schutter (1995) has proposed that LTD induced by PF activation alone plays a role in normalizing the strength of the PF-mediated AMPAR pathway. If PF activation alone is strong enough to induce LTD, the AMPAR pathway is weakened until the Ca^{2+} response reaches the Ca^{2+} threshold. This type of LTD may function as a pretuning process for effective cerebellar learning.

In conclusion, kinetic simulation has allowed us to understand IP_3-dependent Ca^{2+} dynamics, which are capable of coherently explaining various forms of LTD. Because the IP_3-dependent Ca^{2+} threshold, the necessity of PF–CF conjunction, and the PF–CF time delay were reproduced only for physiological ranges of synaptic inputs, the results of this study support conjunctive LTD as one of the cellular bases of cerebellar supervised learning (Marr, 1969; Ito, 1970, 2001; Kawato, 1999).

References

Adkins CE, Taylor CW (1999) Lateral inhibition of inositol 1,4,5-trisphosphate receptors by cytosolic Ca^{2+}. Curr Biol 9:1115–1118.

Aiba A, Kano M, Chen C, Stanton ME, Fox GD, Herrup K, Zwingman TA, Tonegawa S (1994) Deficient cerebellar long-term depression and impaired motor learning in mGluR1 mutant mice. Cell 79:377–388.

Airaksinen MS, Eilers J, Garaschuk O, Thoenen H, Konnerth A, Meyer M (1997) Ataxia and altered dendritic calcium signaling in mice carrying a targeted null mutation of the calbindin D28k gene. Proc Natl Acad Sci USA 94:1488–1493.

Albus JS (1971) A theory of cerebellar function. Math Biosci 10:25–61.

Allbritton NL, Meyer T, Stryer L (1992) Range of messenger action of calcium ion and inositol 1,4,5-trisphosphate. Science 258:1812–1815.

Berridge MJ (1998) Neuronal calcium signaling. Neuron 21:13–26.

Bezprozvanny I, Watras J, Ehrlich BE (1991) Bell-shaped calcium-response curves of $Ins(1,4,5)P_3$- and calcium-gated channels from endoplasmic reticulum of cerebellum. Nature 351:751–754.

Bhalla US, Iyengar R (1999) Emergent properties of networks of biological signaling pathways. Science 283:381–387.

Chen C, Thompson RF (1995) Temporal specificity of long-term depression in parallel fiber-Purkinje synapses in rat cerebellar slice. Learn Mem 2:185–198.

Conquet F, Bashir ZI, Davies CH, Daniel H, Ferraguti F, Bordi F, Franz-Bacon K, Reggiani A, Matarese V, Conde F, Collingridge GL, Crepel F (1994) Motor deficit and impairment of synaptic plasticity in mice lacking mGluR1. Nature 372:237–243.

Daniel H, Levenes C, Crepel F (1998) Cellular mechanisms of cerebellar LTD. Trends Neurosci 21:401–407.

De Schutter E (1995) Cerebellar long-term depression might normalize excitation of Purkinje cells: a hypothesis. Trends Neurosci 18:291–295.

Dupont G, Erneux C (1997) Simulations of the effects of inositol 1,4,5-trisphosphate 3-kinase and 5-phosphatase activities on Ca^{2+} oscillations. Cell Calcium 22:321–331.

Eilers J, Augustine GJ, Konnerth A (1995) Subthreshold synaptic Ca^{2+} signalling in fine dendrites and spines of cerebellar Purkinje neurons. Nature 373:155–158.

Ekerot CF, Kano M (1989) Stimulation parameters influencing climbing fibre induced long-term depression of parallel fibre synapses. Neurosci Res 6:264–268.

Fiala JC, Grossberg S, Bullock D (1996) Metabotropic glutamate receptor activation in cerebellar Purkinje cells as substrate for adaptive timing of the classically conditioned eye-blink response. J Neurosci 16:3760–3774.

Fierro L, Llano I (1996) High endogenous calcium buffering in Purkinje cells from rat cerebellar slices. J Physiol (Lond) 496:617–625.

Fierro L, DiPolo R, Llano I (1998) Intracellular calcium clearance in Purkinje cell somata from rat cerebellar slices. J Physiol (Lond) 510:499–512.

Finch EA, Augustine GJ (1998) Local calcium signalling by inositol-1,4,5-trisphosphate in Purkinje cell dendrites. Nature 396:753–756.

Franks KM, Stevens CF, Sejnowski TJ (2003) Independent sources of quantal variability at single glutamatergic synapses. J Neurosci 23:3186–3195.

Fujiwara A, Hirose K, Yamazawa T, Iino M (2001) Reduced IP_3 sensitivity of IP_3 receptor in Purkinje neurons. NeuroReport 12:2647–2651.

Harris KM, Stevens JK (1988) Dendritic spines of rat cerebellar Purkinje cells: serial electron microscopy with reference to their biophysical characteristics. J Neurosci 8:4455–4469.

Hartell NA (1996) Strong activation of parallel fibers produces localized calcium transients and a form of LTD that spreads to distant synapses. Neuron 16:601–610.

Hartell NA, Furuya S, Jacoby S, Okada D (2001) Intercellular action of nitric oxide increases cGMP in cerebellar Purkinje cells. NeuroReport 12:25–28.

Inoue T, Kato K, Kohda K, Mikoshiba K (1998) Type 1 inositol 1,4,5-trisphosphate receptor is required for induction of long-term depression in cerebellar Purkinje neurons. J Neurosci 18:5366–5373.

Irvine RF, Schell MJ (2001) Back in the water: the return of the inositol phosphates. Nat Rev Mol Cell Biol 2:327–338.

Ito M (1970) Neurophysiological aspects of the cerebellar motor control system. Int J Neurol 7:162–176.

Ito M (2001) Cerebellar long-term depression: characterization, signal transduction, and functional roles. Physiol Rev 81:1143–1195.

Ito M (2002) The molecular organization of cerebellar long-term depression. Nat Rev Neurosci 3:896–902.

Jiang H, Wu D, Simon MI (1994) Activation of phospholipase C β4 by heterotrimeric GTP-binding proteins. J Biol Chem 269:7593–7596.

Karachot L, Kado RT, Ito M (1994) Stimulus parameters for induction of long-term depression in *in vitro* rat Purkinje cells. Neurosci Res 21:161–168.

Kawato M (1999) Internal models for motor control and trajectory planning. Curr Opin Neurobiol 9:718–727.

Khodakhah K, Ogden D (1995) Fast activation and inactivation of inositol trisphosphate-evoked Ca^{2+} release in rat cerebellar Purkinje neurones. J Physiol (Lond) 487:343–358.

Kim JJ, Thompson RF (1997) Cerebellar circuits and synaptic mechanisms involved in classical eyeblink conditioning. Trends Neurosci 20:177–181.

Klingauf J, Neher E (1997) Modeling buffered Ca^{2+} diffusion near the membrane: implications for secretion in neuroendocrine cells. Biophys J 72:674–690.

Kuroda S, Schweighofer N, Kawato M (2001) Exploration of signal transduction pathways in cerebellar long-term depression by kinetic simulation. J Neurosci 21:5693–5702.

Linden DJ, Connor JA (1995) Long-term synaptic depression. Annu Rev Neurosci 18:319–357.

Llinas R, Lang EJ, Welsh JP (1997) The cerebellum, LTD, and memory: alternative views. Learn Mem 3:445–455.

Luzzi V, Sims CE, Soughayer JS, Allbritton NL (1998) The physiologic concentration of inositol 1,4,5-trisphosphate in the oocytes of *Xenopus laevis*. J Biol Chem 273:28657–28662.

MacGregor RJ (1987) Neural and brain modeling. San Diego: Academic.

Maeda H, Ellis-Davies GC, Ito K, Miyashita Y, Kasai H (1999) Supralinear Ca^{2+} signaling by cooperative and mobile Ca^{2+} buffering in Purkinje neurons. Neuron 24:989–1002.

Marchant JS, Taylor CW (1997) Cooperative activation of IP_3 receptors by sequential binding of IP_3 and Ca^{2+} safeguards against spontaneous activity. Curr Biol 7:510–518.

Marr D (1969) A theory of cerebellar cortex. J Physiol (Lond) 202:437–470.

Mateos JM, Benitez R, Elezgarai I, Azkue JJ, Lazaro E, Osorio A, Bilbao A, Donate F, Sarria R, Conquet F, Ferraguti F, Kuhn R, Knopfel T, Grandes P (2000) Immunolocalization of the mGluR1b splice variant of the metabotropic glutamate receptor 1 at parallel fiber-Purkinje cell synapses in the rat cerebellar cortex. J Neurochem 74:1301–1309.

Miyakawa H, Lev-Ram V, Lasser-Ross N, Ross WN (1992) Calcium transients evoked by climbing fiber and parallel fiber synaptic inputs in guinea pig cerebellar Purkinje neurons. J Neurophysiol 68:1178–1189.

Miyata M, Finch EA, Khiroug L, Hashimoto K, Hayasaka S, Oda SI, Inouye M, Takagishi Y, Augustine GJ, Kano M (2000) Local calcium release in dendritic spines required for long-term synaptic depression. Neuron 28:233–244.

Rose CR, Konnerth A (2001) Stores not just for storage. Intracellular calcium release and synaptic plasticity. Neuron 31:519–522.

Sabatini BL, Svoboda K (2000) Analysis of calcium channels in single spines using optical fluctuation analysis. Nature 408:589–593.

Sabatini BL, Oertner TG, Svoboda K (2002) The life cycle of Ca^{2+} ions in dendritic spines. Neuron 33:439–452.

Schreurs BG, Oh MM, Alkon DL (1996) Pairing-specific long-term depression of Purkinje cell excitatory postsynaptic potentials results from a classical conditioning procedure in the rabbit cerebellar slice. J Neurophysiol 75:1051–1060.

Stuart G, Hausser M (1994) Initiation and spread of sodium action potentials in cerebellar Purkinje cells. Neuron 13:703–712.

Sugiyama T, Hirono M, Suzuki K, Nakamura Y, Aiba A, Nakamura K, Nakao K, Katsuki M, Yoshioka T (1999) Localization of phospholipase Cβ isozymes in the mouse cerebellum. Biochem Biophys Res Commun 265:473–478.

Tanaka J, Nakagawa S, Kushiya E, Yamasaki M, Fukaya M, Iwanaga T, Simon MI, Sakimura K, Kano M, Watanabe M (2000) G_q protein alpha subunits $G\alpha_q$ and $G\alpha_{11}$ are localized at postsynaptic extra-junctional membrane of cerebellar Purkinje cells and hippocampal pyramidal cells. Eur J Neurosci 12:781–792.

Vecellio M, Schwaller B, Meyer M, Hunziker W, Celio MR (2000) Alterations in Purkinje cell spines of calbindin D-28 k and parvalbumin knockout mice. Eur J Neurosci 12:945–954.

Vetter P, Roth A, Hausser M (2001) Propagation of action potentials in dendrites depends on dendritic morphology. J Neurophysiol 85:926–937.

Wang SS, Denk W, Hausser M (2000) Coincidence detection in single dendritic spines mediated by calcium release. Nat Neurosci 3:1266–1273.

Xu T, Naraghi M, Kang H, Neher E (1997) Kinetic studies of Ca^{2+} binding and Ca^{2+} clearance in the cytosol of adrenal chromaffin cells. Biophys J 73:532–545.

Yamamoto K, Kobayashi Y, Takemura A, Kawano K, Kawato M (2002) Computational studies on acquisition and adaptation of ocular following responses based on cerebellar synaptic plasticity. J Neurophysiol 87:1554–1571.